Supporting Information for

Mechanochemical Synthesis of Methylammonium Lead Mixed–Halide Perovskites: Unraveling the Solid-Solution Behavior using Solid-State NMR

*Abhoy Karmakar,[1§] Abdelrahman M. Askar,[2§] Guy M. Bernard,[1] Victor V. Terskikh,[3] Michelle Ha,[1] Sahil Patel,[2] Karthik Shankar,[2,4] and Vladimir K. Michaelis[1]**

1-Department of Chemistry, University of Alberta, Edmonton, Alberta, Canada, T6G 2G2

2-Department of Electrical and Computer Engineering, University of Alberta, Edmonton,
Alberta, Canada, T6G 1H9

3- Department of Chemistry, University of Ottawa, Ottawa, Ontario, Canada, K1N 6N5

4-NRC National Institute for Nanotechnology, Edmonton, Alberta, Canada, T6G 2M9

[§] co-authors contributed equally

[*]Corresponding author: vladimir.michaelis@ualberta.ca

TABLE OF CONTENTS

CONTENT	PAGE #
Table S1: ^{207}Pb NMR linewidth (FWHM) of $MAPbX_3$	S4
Table S2: DFT quantum chemical calculations (ADF) on $[PbCl_xBr_{6-x}]^{4-}$ anions	S4
Table S3: Spin-spin relaxation time (T_2) of parent and 50/50 MHP	S5
Table S4: DFT GIPAW periodic-based quantum chemical calculations (CASTEP)	S5
Table S5: Elemental atomic ratios for the MHP samples determined using the EDX technique	S6
Figure S1. ^{207}Pb NMR spectrum of an MAS sample of $MAPb(Cl_{0.05}Br_{0.95})_3$ acquired at 7.05 T with a spinning frequency of 13 kHz.	S7
Figure S2. ^{207}Pb NMR spectra of an MAS sample of $MAPb(Cl_{0.95}Br_{0.05})_3$ acquired at 11.7 T and at 7.05 T.	S7
Deconvolution of ^{207}Pb NMR Spectra	S8
Figure S3. Simulated ^{207}Pb NMR spectra for (a) $MAPb(Cl_{0.25}Br_{0.75})_3$ (b) $MAPb(Cl_{0.5}Br_{0.5})_3$ and for (c) $MAPb(Cl_{0.75}Br_{0.25})_3$	S8
Table S6: Probabilities for the $[PbCl_xBr_{6-x}]^{4-}$ anions	S9
Table S7: Percent contribution to the total area of the ^{207}Pb NMR spectra for MHPs from a given $[PbCl_xBr_{6-x}]^{4-}$ unit. Spectra acquired at 11.7 T.	S10
Figure S4. Unit cell expansion with the change in ^{207}Pb δ_{cs} as Br replaces Cl	S11
Figure S5. Relationship between MHPs physical properties (Band gap (Eg) & electronegativity (χ_p)) with atomic structure from x-ray diffraction (unit cell parameter, a (Å)) and NMR spectroscopy (chemical shift, $\delta(^{207}Pb)$/ppm).	S12
Figure S6. Diffuse reflectance spectra for MCS-HG $MAPb(Cl_xBr_{1-x})_3$, with x = 0.75, 0.50, and 0.25, along with those for their parent compounds, $MAPbBr_3$ and $MAPbCl_3$.	S13
Figure S7. Comparison of DFT calculated isotropic ^{207}Pb shielding parameter (ppm) for Cl/Br substituted $[PbX_xX'_{6-x}]^{4-}$ octahedra using a 2 × 2 × 2 supercell	S14
Figure S8. Powder XRD pattern for $MAPb(Cl_{0.5}Br_{0.5})_3$ prepared using the SS method.	S15
Figure S9. ^{207}Pb NMR spectra for non-spinning $MAPb(Cl_xBr_{1-x})_3$ (x = 0.25, 0.50, 0.75) acquired at 7.05 T, prepared by using the MCS-BM method for 1 hr.	S16

Figure S10. FESEM images for the MHP samples prepared by SS, MCS-HG and MCS-BM.	S17
Figure S11. FESEM images for MCS-BM MHP sample MAPb($Cl_{0.5}Br_{0.5}$) high (left, 200 nm) and low (right, 2 μm) magnification.	S18
Figure S12. ^{1}H MAS NMR spectra of MAPb($Cl_{0.5}Br_{0.5}$)$_3$ (BM, HG, SS)	S18
Figure S13. ^{13}C CP MAS NMR spectra of MAPb($Cl_{0.5}Br_{0.5}$)$_3$ (BM, HG, SS)	S19
Figure S14. ^{207}Pb NMR spectra for non-spinning MAPb($Cl_{0.75}Br_{0.25}$)$_3$, prepared by using the MCS-BM method for 5 mins and 1 hr together with XRD pattern of the same sample	S19
Figure S15. Diffuse reflectance spectra for MAPb($Cl_{0.5}Br_{0.5}$)$_3$ prepared by BM, HG, and SS, along with those for the parent compounds, $MAPbBr_3$ and $MAPbCl_3$.	S20
Figure S16. Comparison between XRD patterns of MAPb($Br_{0.5}I_{0.5}$)$_3$ prepared by MCS-HG (2 hrs) and their parent compounds, $MAPbI_3$ and $MAPbBr_3$.	S20
Figure S17. Diffuse reflectance plots of the MAPb($Br_{0.5}I_{0.5}$)$_3$ sample prepared by MCS-HG (2 hrs), along with those for the parent compounds, $MAPbBr_3$ and $MAPbI_3$.	S21
References	S21

Table S1: ^{207}Pb NMR linewidth (FWHM) of $MAPbX_3$

$MAPbX_3$	FWHM (Hz) non-spinning, 21.1 T	FWHM (Hz) non-spinning, 7.05 T[a]	FWHM (Hz) MAS, 14.1 T[a]	FWHM (Hz) MAS, 14.1 T[b]
X = Cl	3,700	3,700	3,000	3,000
X = Br	15,000	15,300	17,000	15,900
X = I	25,500	19,800	30,500	21,100

a. See Ref. [1]; b. See Ref. [2]

Table S2: DFT quantum chemical calculations (ADF) on $[PbCl_xBr_{6-x}]^{4-}$ anions

Environment	σ_{iso} (ppm)	δ_{iso} (ppm)[a]	Ω (ppm)	κ
$[PbCl_6]^{4-}$	9538	−914	0.0	0.00
$[PbCl_5Br]^{4-}$	9300	−675	282	1.00
trans-$[PbCl_4Br_2]^{4-}$	9084	−460	537	1.00
cis-$[PbCl_4Br_2]^{4-}$	9082	−458	283	−0.57
mer-$[PbCl_3Br_3]^{4-}$	8890	−266	470	0.09
fac-$[PbCl_3Br_3]^{4-}$	8881	−257	92	−1.00
trans-$[PbCl_2Br_4]^{4-}$	8736	−112	354	−1.00
cis-$[PbCl_2Br_4]^{4-}$	8709	−85	252	0.51
$[PbClBr_5]^{4-}$	8584	41	149	−1.00
$[PbBr_6]^{4-}$	8534	90	0.0	0.00

[a] $\delta_{iso,calc}$ (ppm) = $-(\sigma_{iso,calc} - 8858.4$ ppm).

Table S3: Spin-spin relaxation time (T_2) of parent and 50/50 MCS MHP

Sample	$[PbBr_6]^{4-}$	$[PbClBr_5]^{4-}$	$[PbCl_2Br_4]^{4-}$	$[PbCl_3Br_3]^{4-}$	$[PbCl_4Br_2]^{4-}$	$[PbCl_5Br]^{4-}$	$[PbCl_6]^{4-}$
$MAPb(Cl_{0.5}Br_{0.5})_3$ (µs)	54[a]	57 [a]		66 [a]	93 [a]		98 [a]
$MAPbCl_3$ (µs)	-	-		-	-		150[b] 75[c] 321[d]
$MAPbBr_3$ (µs)	70[c] 63[d]	-		-	-		-

a. 21.1 T, (T_2, spin-echo, non-spinning); b. 11.75 T, (T_2, spin-echo, non-spinning); c. See Ref. 1 (T_2*, MAS, 14.1 T); d. See Ref. 2 (T_2, spin-echo, non-spinning, 9.4 T)

Table S4: DFT GIPAW periodic-based quantum chemical calculations (CASTEP)

Environment	σ_{iso} (ppm)	Ω (ppm)	κ
$[PbCl_6]^{4-}$	5799	0.1	−0.68
$[PbCl_5Br]^{4-}$	5514	428	−1.00
$[PbCl_4Br_2]^{4-}$	5217	44	1.00
$[PbCl_4Br_2]^{4-}$	5195	894	−1.00
$[PbCl_3Br_3]^{4-}$	4886	924	−0.01
$[PbCl_3Br_3]^{4-}$	4909	1.4	−0.98
$[PbCl_2Br_4]^{4-}$	4564	480	−0.99
$[PbCl_2Br_4]^{4-}$	4545	946	1.00
$[PbClBr_5]^{4-}$	4209	483	1.00
$[PbBr_6]^{4-}$	3842	0.04	0.15

Table S5: Elemental atomic ratios for the MHP samples determined using the EDX technique.

Sample	Cl (atomic %)	Br (atomic %)	Ratio	Cl+Br (X) (atomic %)	Pb (atomic %)	X:Pb
$MAPb(Cl_{0.25}Br_{0.75})_3$ – HG	5.8	19.2	1:3.3	25	8.8	2.8:1
$MAPb(Cl_{0.50}Br_{0.50})_3$ – HG	10.8	10.4	1.03:1	21.2	7.7	2.8:1
$MAPb(Cl_{0.75}Br_{0.25})_3$ – HG	5.9	1.9	3.01:1	7.8	2.7	2.8:1
$MAPb(Cl_{0.50}Br_{0.50})_3$ – BM	7.3	8.0	1:1.09	15.3	5.5	2.8:1
$MAPb(Cl_{0.50}Br_{0.50})_3$ – SS	6.94	5.0	1.38:1	11.9	5.12	2.3:1

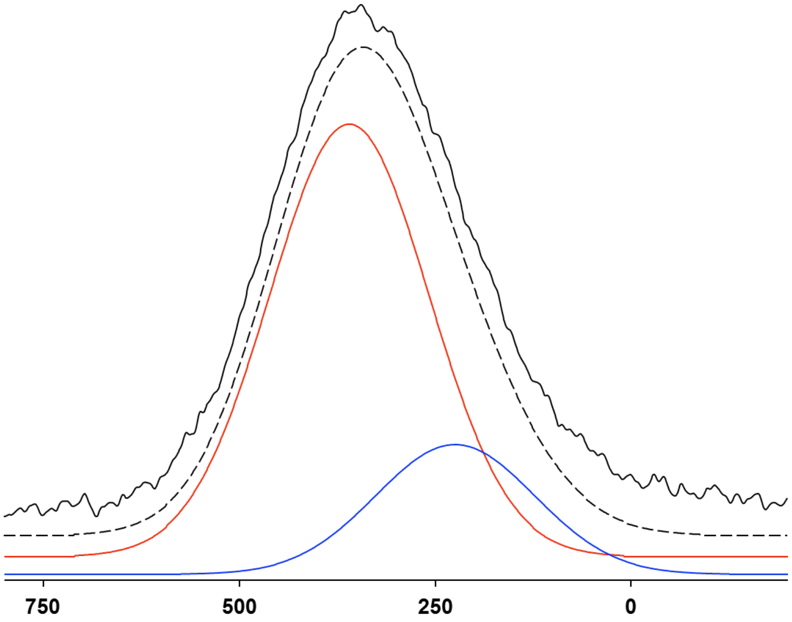

Figure S1: ^{207}Pb NMR spectrum of an MAS sample of MAPb(Cl$_{0.05}$Br$_{0.95}$)$_3$ acquired at 7.05 T with a spinning frequency of 13 kHz (upper trace). The dashed line is the simulated spectrum and is the sum of a site at δ_{CS} = 360 ppm (red trace) and at δ_{CS} = 225 ppm (blue trace). The latter has 30 % the intensity of the former.

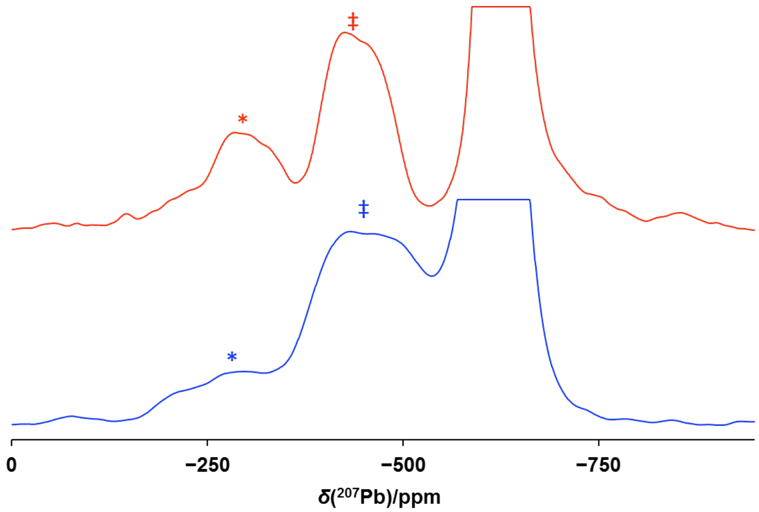

Figure S2: ^{207}Pb NMR spectra of an MAS sample of MAPb(Cl$_{0.95}$Br$_{0.05}$)$_3$ acquired at 11.7 T at 13.5 kHz (upper red trace) and at 7.05 T with a spinning frequency of 13 kHz (lower, blue trace). The truncated peak is attributed to [PbCl$_6$]$^{4-}$ units—see Figure 2 of the manuscript for a full spectrum of the sample acquired at 11.7 T. The peaks marked with ‡ are attributed to [PbCl$_5$Br$_1$]$^{4-}$ units. The asterisks indicate spinning side bands.

Deconvolution of ^{207}Pb NMR Spectra

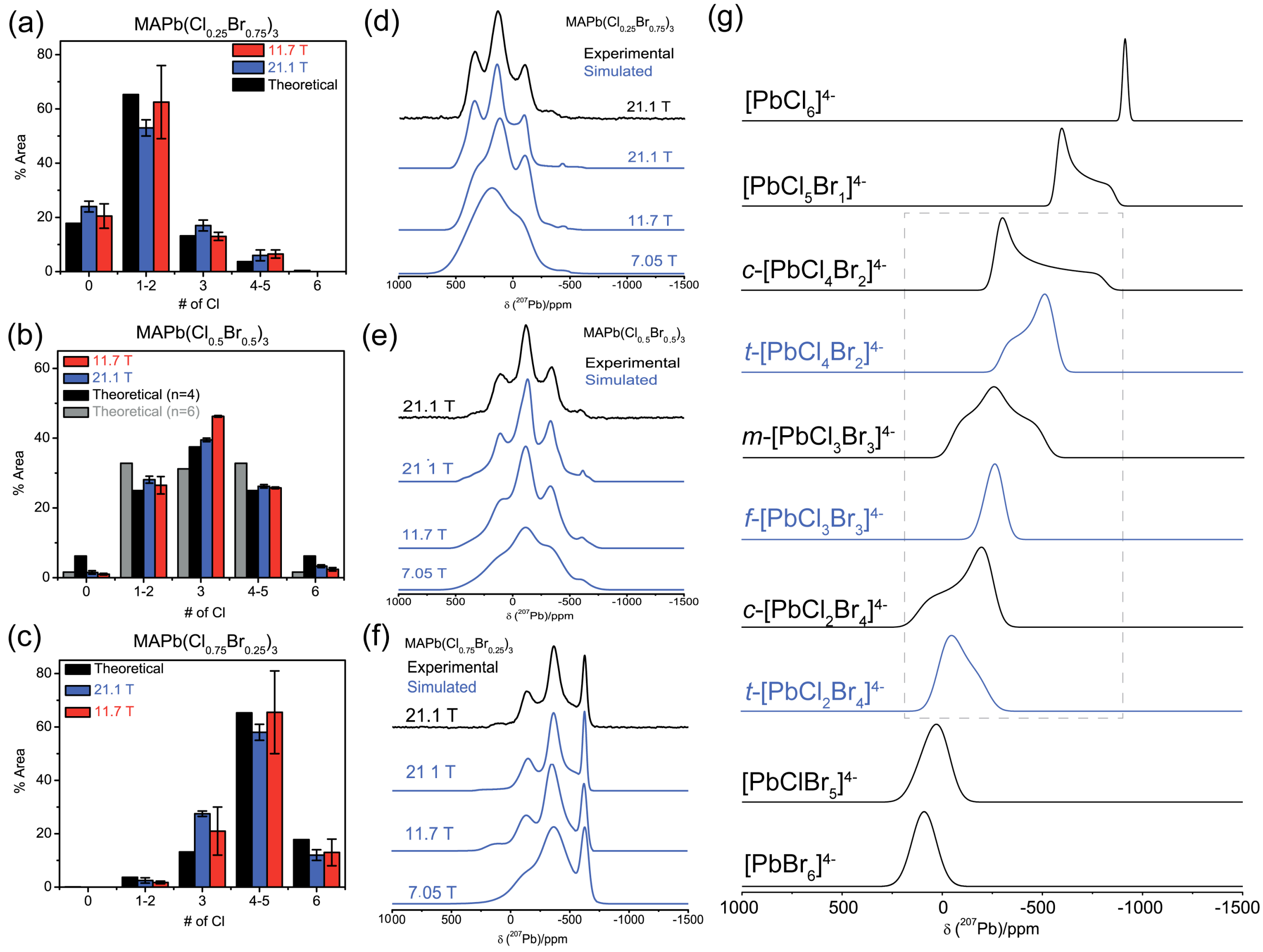

Figure S3: Simulated ^{207}Pb NMR spectra for (a) $MAPb(Cl_{0.25}Br_{0.75})_3$ (b) $MAPb(Cl_{0.5}Br_{0.5})_3$ and for (c) $MAPb(Cl_{0.75}Br_{0.25})_3$ acquired at the indicated fields fit according to the population distributions indicated by the bar charts, following a binomial-like distribution based on Gaussians. Data were further fit (d-f) using insight from the DFT calculated shielding parameters (g) determined using ADF on model anions, whereby the site distribution of seven unique Pb environments were fixed at a binomial distribution and slight changes to the CSA parameters were implemented to obtain best overall fits. Errors were assessed using the Gaussian fitting procedure at multiple field strengths. NB: c = cis; t = trans; f = fac & m= mer.

In principle, a ^{207}Pb NMR spectrum for a MHP of the type $[PbX_xX`_{6-x}]^{4-}$ ($0 < x < 6$) may consist of 10 distinct sites arising from the isomers summarized in Table S6. In fact, as discussed in the manuscript, only seven distinct peak maxima were identified. These have been attributed to one each of the seven possible $[PbCl_xBr_{6-x}]^{4-}$ octahedra, with the assumption that the chemical shift difference between each pair of geometric isomers (e.g., *cis*- and *trans*-$[PbCl_4Br_2]^{4-}$) is not resolved because of the moderate field strength used here and because there is significant overlap for these sites. Our calculations support this conclusion, with differences between geometric isomers ≤ 27 ppm (see Table S2) compared to an average chemical shift difference between distinct anion units of greater than 160 ppm. Experimental data for the $[PbCl_xBr_{6-x}]^{4-}$ anions are not available, but studies on a series of $[PtCl_xBr_{6-x}]^{2-}$ anions are instructive.[3,4] As for ^{207}Pb, the coordination about the ^{195}Pt is octahedral, and the ^{195}Pt chemical shift is even more sensitive to its environment than that for ^{207}Pb. For example, the chemical shift difference between $[PtCl_6]^{2-}$ and $[PtBr_6]^{2-}$ is almost 1900 ppm,[3,4] compared to approximately 1000 ppm for the corresponding ^{207}Pb anions. Nevertheless, these groups both report chemical shift differences of 3 ppm or less between each of the three pairs of geometric isomers.

Table S6. Probabilities for the $[PbCl_xBr_{6-x}]^{4-}$ anions.[a]

Isomer	Probability/%[a]
$[PbCl_6]^{4-}$	100
$[PbCl_5Br_1]^{4-}$	100
t-$[PbCl_4Br_2]^{4-}$	50
c-$[PbCl_4Br_2]^{4-}$	50
m-$[PbCl_3Br_3]^{4-}$	50
f-$[PbCl_3Br_3]^{4-}$	50
t-$[PbCl_2Br_4]^{4-}$	50
c-$[PbCl_2Br_4]^{4-}$	50
$[PbCl_1Br_5]^{4-}$	100
$[PbBr_6]^{4-}$	100

a. Probabilities listed here are those expected in the absence of thermodynamic or other governing factors.

b. c = cis; t = trans; f = fac & m= mer

Although seven distinct peak maxima were identified (Table 1), the anions, apart from $[PbCl_6]^{4-}$ and $[PbBr_6]^{4-}$, are subject to CSA. Thus, a further complication is that the geometric isomers are predicted to have different lineshapes, Figure S3g (but similar chemical shifts, as discussed above). Since the spans of these sites are greater than the chemical shift differences between neighboring sites, there is significant overlap, rendering it impossible to isolate the contributions from separate sites. For the simulations, initial populations were based on the theoretical values obtained from the assumption of a binomial distribution, and initial lineshapes were based on the calculated values (Table S2). These were adjusted to obtain simulated spectra that best fit experimental spectra, as illustrated in Figure S3d-f. To compare the agreement between the fits of the experimental data and those expected on the basis of computational results, the areas under five regions were determined; these are summarized in Table S7.

Table S7: Percent contribution to the total area of the ^{207}Pb NMR spectra for MHPs from a given $[PbCl_xBr_{6-x}]^{4-}$ unit. Spectra acquired at 11.75 T.

Samples		**$[PbBr_6]^{4-}$**	**$[PbClBr_5]^{4-}$ + $[PbCl_2Br_4]^{4-}$**	**$[PbCl_3Br_3]^{4-}$**	**$[PbCl_4Br_2]^{4-}$ + $[PbCl_5Br]^{4-}$**	**$[PbCl_6]^{4-}$**
$MAPbBr_3$	Theoretical[a] (%)	100	0	0	0	0
	Experimental[b] (%)	100	0	0	0	0
$MAPb(Cl_{0.05}Br_{0.95})_3$	Theoretical[a] (%)	73.5	26.3	0.2	0	0
	Experimental[b] (%)	72 (5)	28 (5)	0	0	0
$MAPb(Cl_{0.25}Br_{0.75})_3$[4]	Theoretical[a] (%)	17.8	65.3	13.2	3.7	0
	Experimental[b] (%)	20.5 (5)	61.5 (14)	13 (3)	6.5 (2)	0
$MAPb(Cl_{0.50}Br_{0.50})_3$[4]	Theoretical[a] (%)	1.6	32.8	31.2	32.8	1.6
	Experimental[b] (%)	1.5 (1)	21 (5)	50 (10)	27 (5)	1 (1)
$MAPb(Cl_{0.75}Br_{0.25})_3$[4]	Theoretical[a] (%)	0	3.7	13.3	65.3	17.8
	Experimental[b] (%)	0	1.75 (1)	21 (9)	65.5 (17)	13 (5)
$MAPb(Cl_{0.95}Br_{0.05})_3$	Theoretical[a] (%)	0	0	0.2	26.3	73.5
	Experimental[b] (%)	0	0	0	28 (2)[c]	72 (2)[c]
$MAPbCl_3$	Theoretical[a] (%)	0	0	0	0	100
	Experimental[b] (%)	0	0	0	0	100

a. Theoretical binomial distribution for seven sites (n=6), using Gaussians as a first approximation.

b. Experimental results based on 11.75 T.

c. Assessed from MAS NMR experiments at 7.05 and 11.75 T.

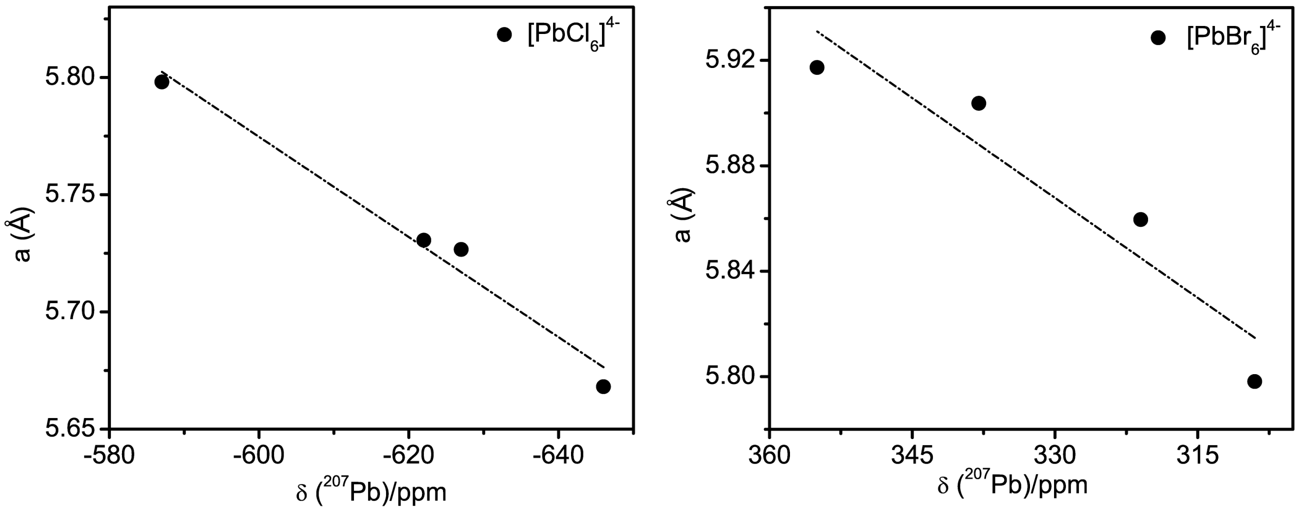

Figure S4. Sensitivity of experimental δ_{cs}(^{207}Pb) for $[PbCl_6]^{4-}$ (left) and $[PbBr_6]^{4-}$ (right) as the unit cell changes (*a* = *b* = *c*) to accommodate halide mixing.

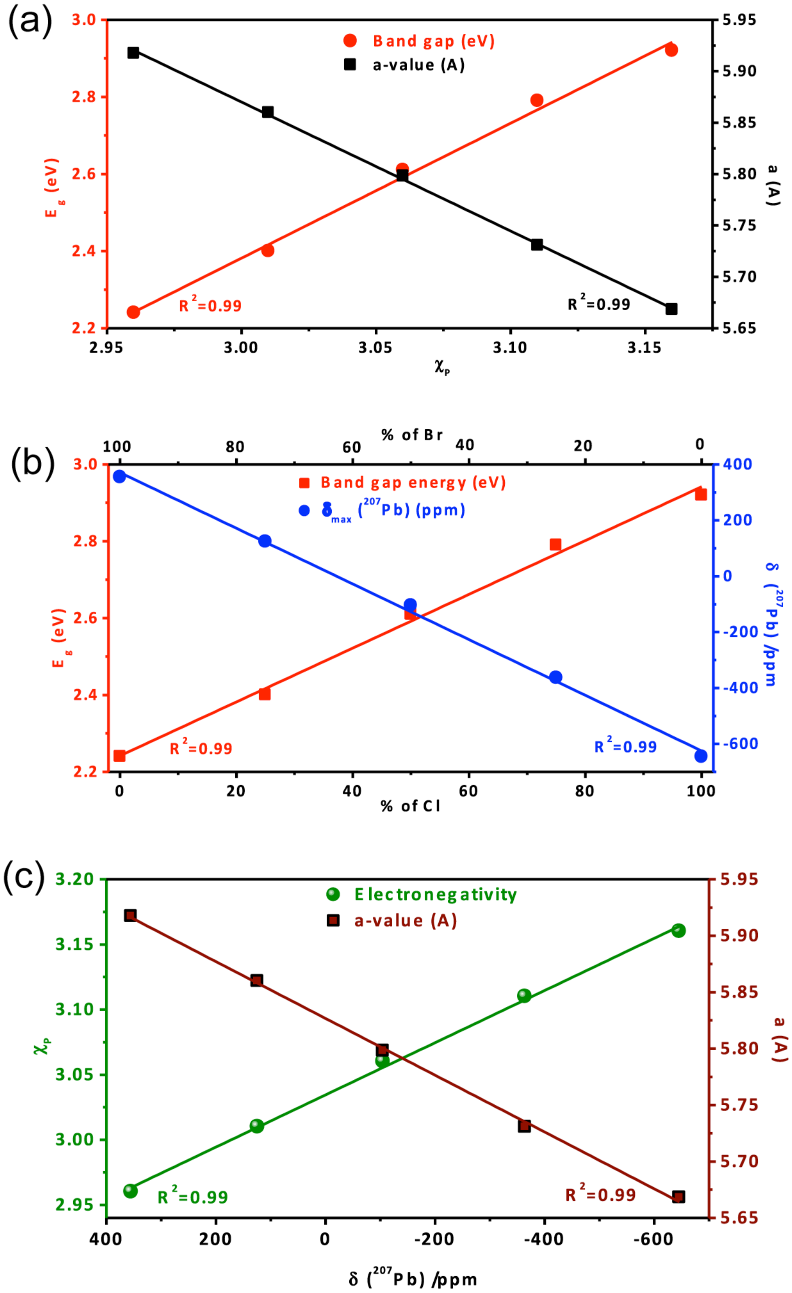

Figure S5. Relationship between MHP physical properties (Band gap (*E*g)) and electronegativity ($\chi_p;\chi_p=\sum_1 a(i)\chi(i)$) where *a*(i) = fraction of halide 'i' (Cl or Br) and χ(i) = Pauling electronegativity of halide 'i' (χ(Cl) or χ(Br)) with atomic structure from X-ray diffraction (unit cell parameter, *a* (Å)) and NMR spectroscopy (chemical shift, δ(^{207}Pb)/ppm).

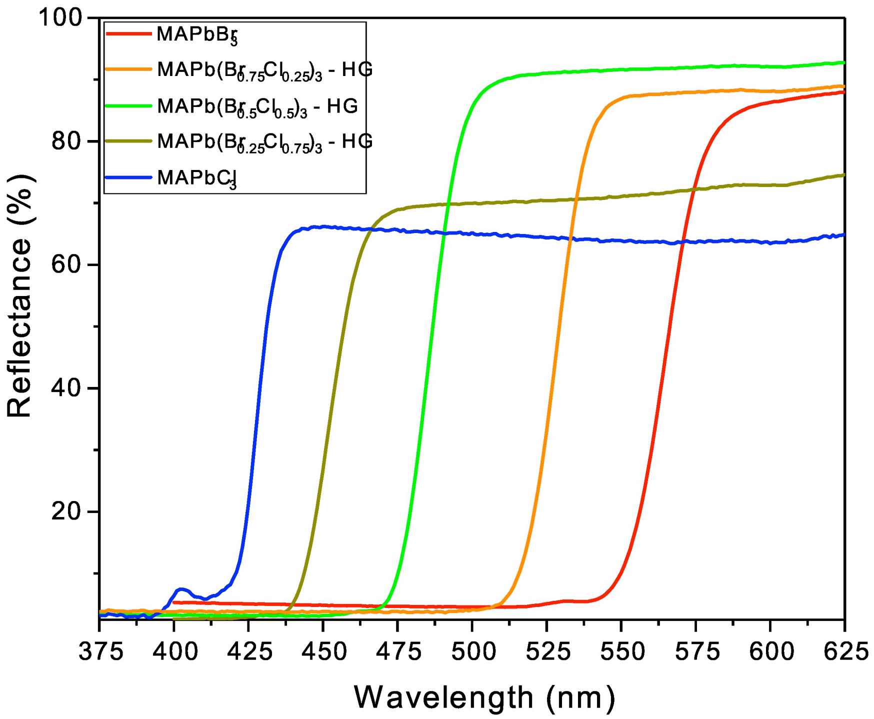

Figure S6. Diffuse reflectance spectra for MCS-HG MAPb(Cl_xBr_{1-x})$_3$, with x = 0.75, 0.50, and 0.25, along with those for their parent compounds, $MAPbBr_3$ and $MAPbCl_3$.

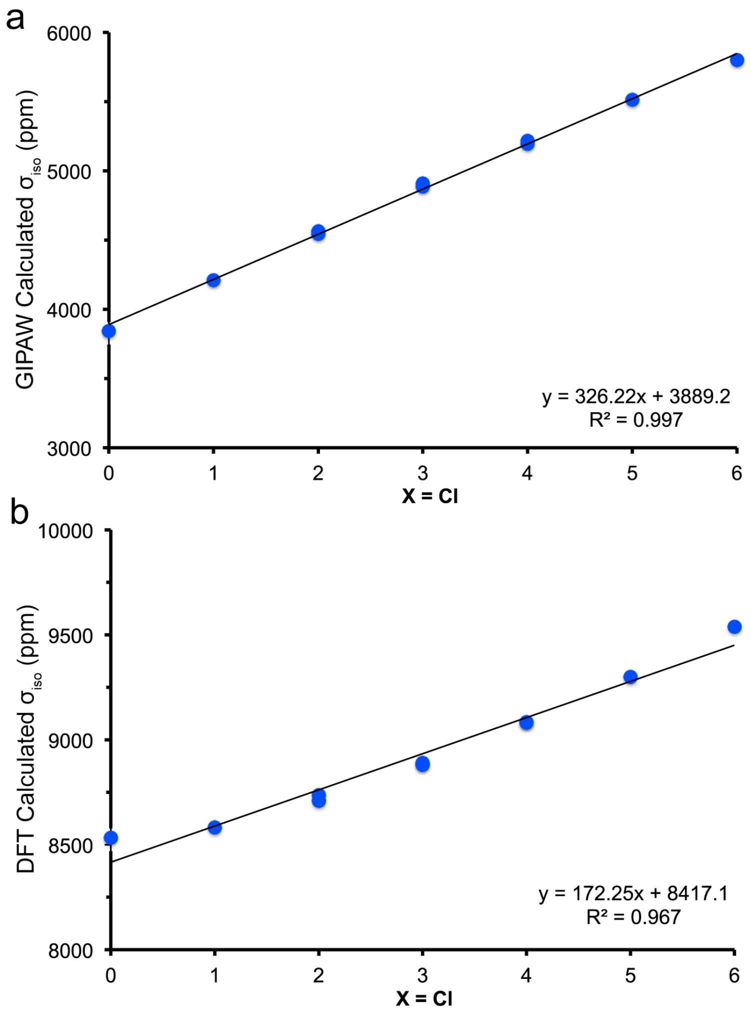

Figure S7. Comparison of DFT calculated isotropic ^{207}Pb shielding parameter (ppm) on Cl/Br substituted $[PbX_xX'_{6-x}]^{4-}$ octahedra using a 2 x 2 x 2 supercell (GIPAW) as implemented in CASTEP (a) or on a model anion as implemented in ADF (b).

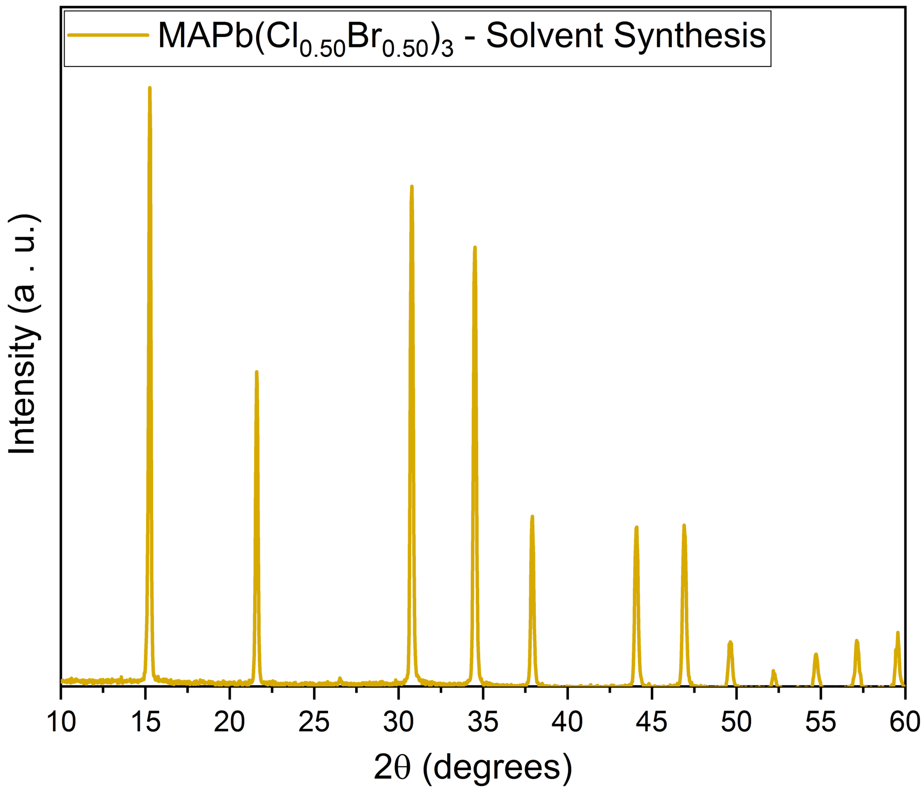

Figure S8. Powder XRD pattern for MAPb(Cl$_{0.5}$Br$_{0.5}$)$_3$ prepared using the SS method.

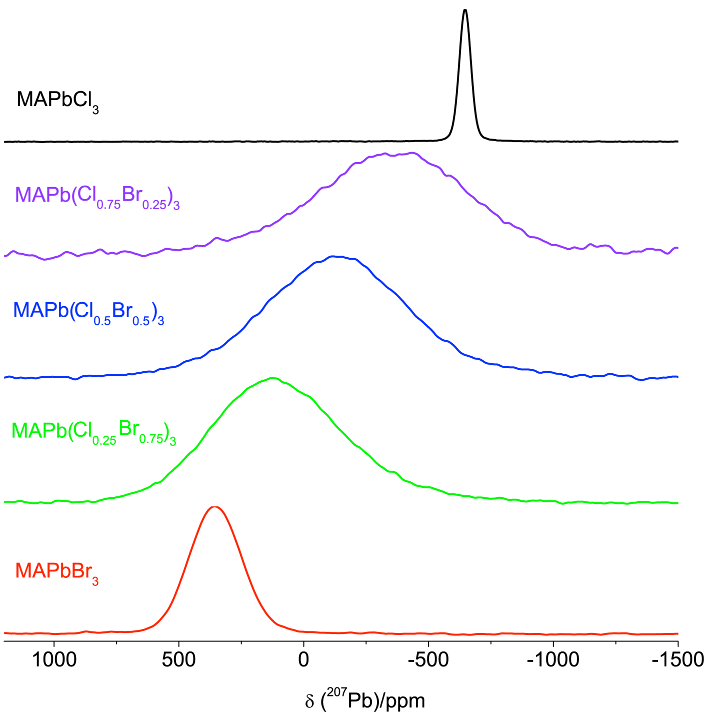

Figure S9. **^{207}Pb NMR spectra for non-spinning MAPb(Cl$_x$Br$_{1-x}$)$_3$, where x = 0, 0.25, 0.50, 0.75 and 1. MCS-BM method was used to prepare MHPs (purple, blue and green). Samples were ball milled for a period of 1 hr. All spectra were acquired at 7.05 T.**

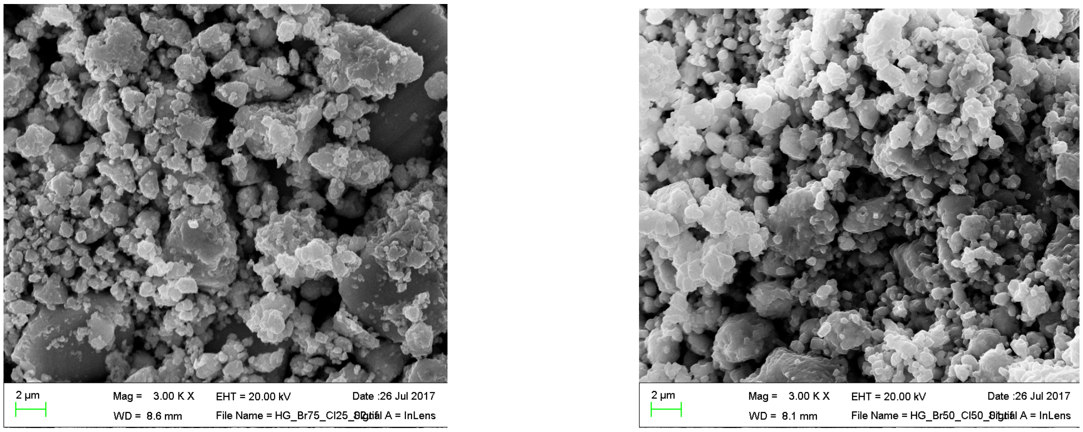

(a) $MAPb(Cl_{0.25}Br_{0.75})_3$ – HG **(b) $MAPb(Cl_{0.5}Br_{0.5})_3$ – HG**

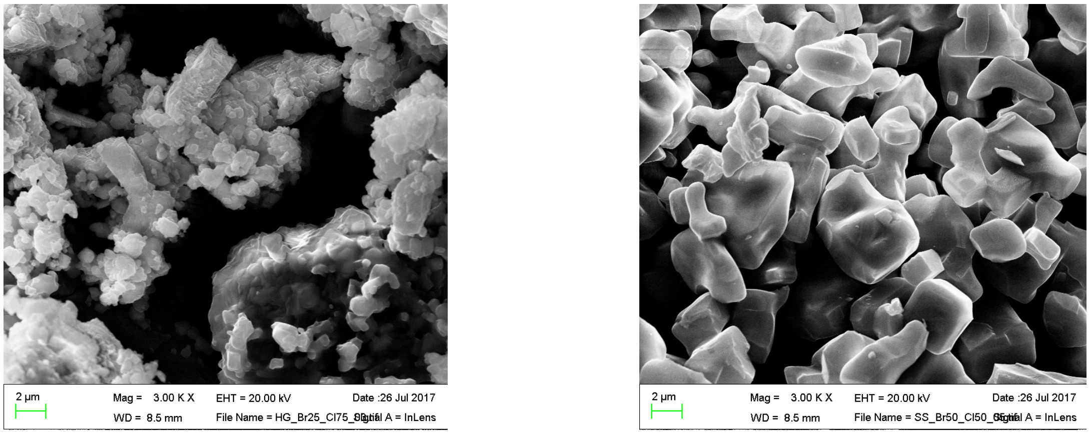

(c) $MAPb(Cl_{0.75}Br_{0.25})_3$ – HG **(d) $MAPb(Cl_{0.5}Br_{0.5})_3$ – SS**

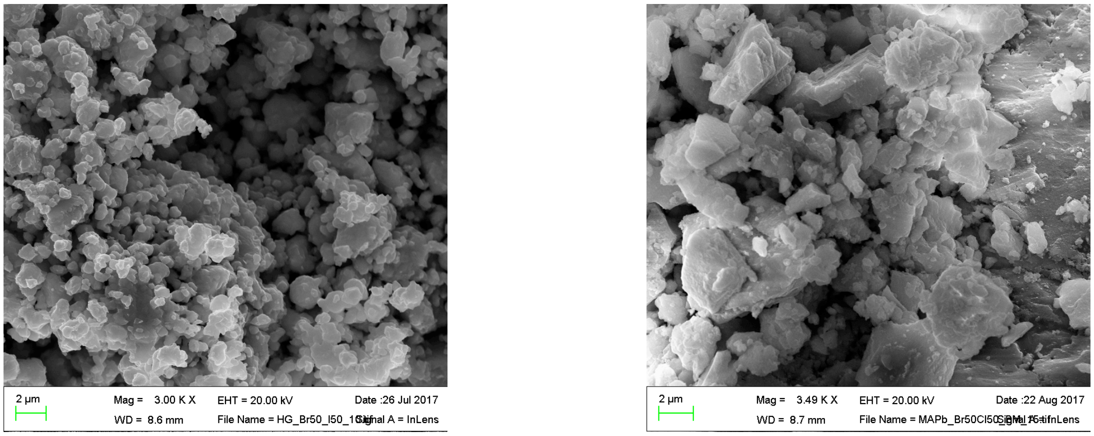

(e) $MAPb(Cl_{0.5}Br_{0.5})_3$ – HG **(f) $MAPb(Cl_{0.5}Br_{0.5})_3$ – BM**

Figure S10. FESEM images for the MHP samples prepared by SS, MCS-HG and MCS-BM.

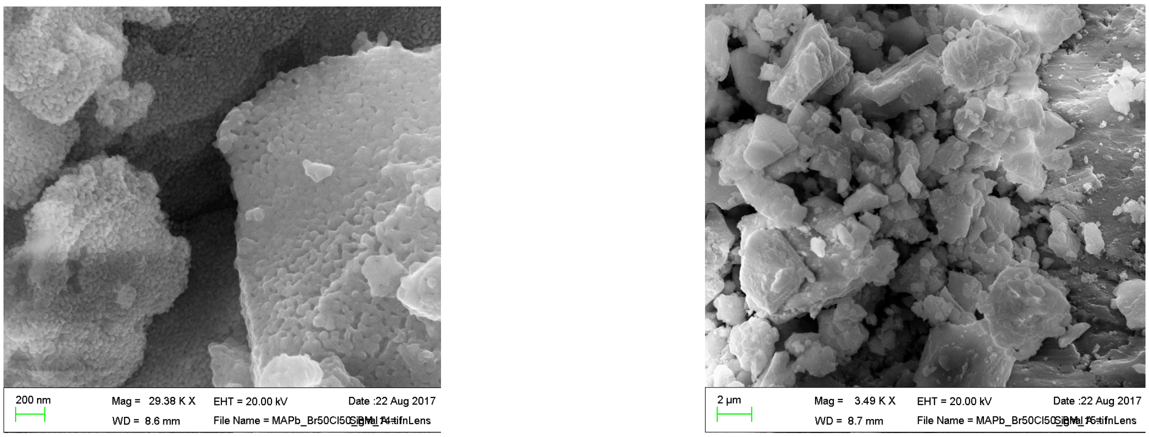

Figure S11. FESEM images for MCS-BM MHP sample MAPb($Cl_{0.5}Br_{0.5}$) high (left, 200 nm) and low (right, 2 µm) magnification.

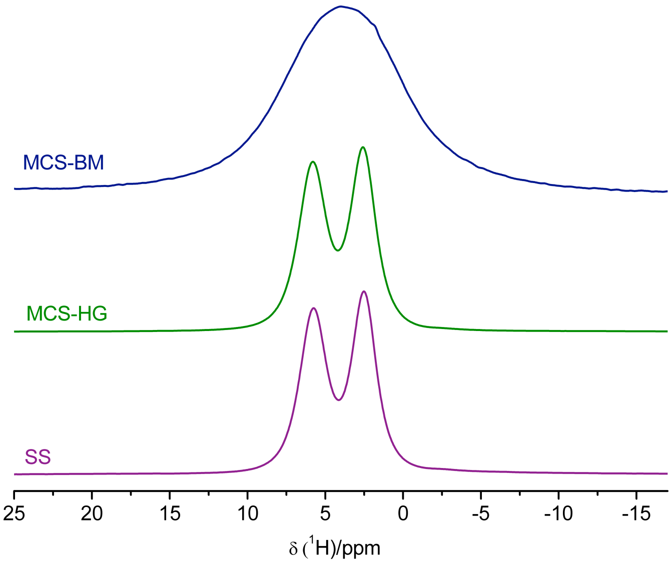

Figure S12. ^{1}H NMR spectra of MAPb($Cl_{0.5}Br_{0.5}$)$_3$ samples acquired at 7.05 T with 10 kHz MAS; samples prepared by the indicated techniques.

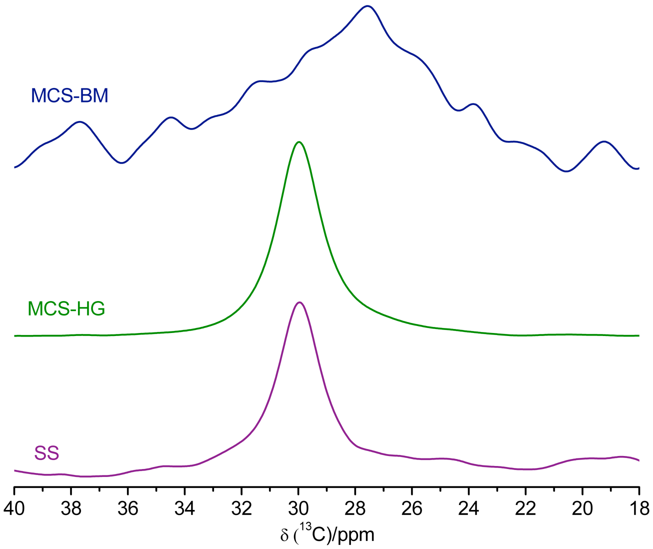

Figure S13. ^{13}**C CP NMR spectra of** $MAPb(Cl_{0.5}Br_{0.5})_3$ **samples, obtained at 7.05 T with 10 kHz MAS. The samples were prepared by the indicated techniques.**

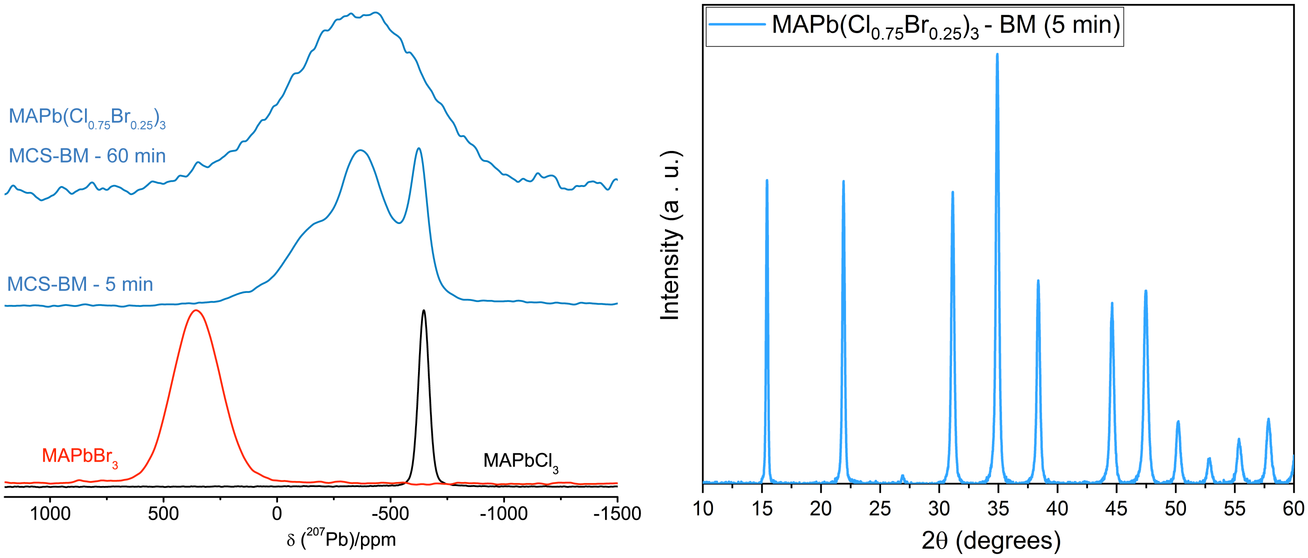

Figure S14. ^{207}**Pb NMR spectra of non-spinning** $MAPb(Cl_{0.75}Br_{0.25})_3$**, prepared by using the MCS-BM method for 5 min and 1 hr (left) and XRD pattern, obtained after using the MCS-BM method for 5 min (right).**

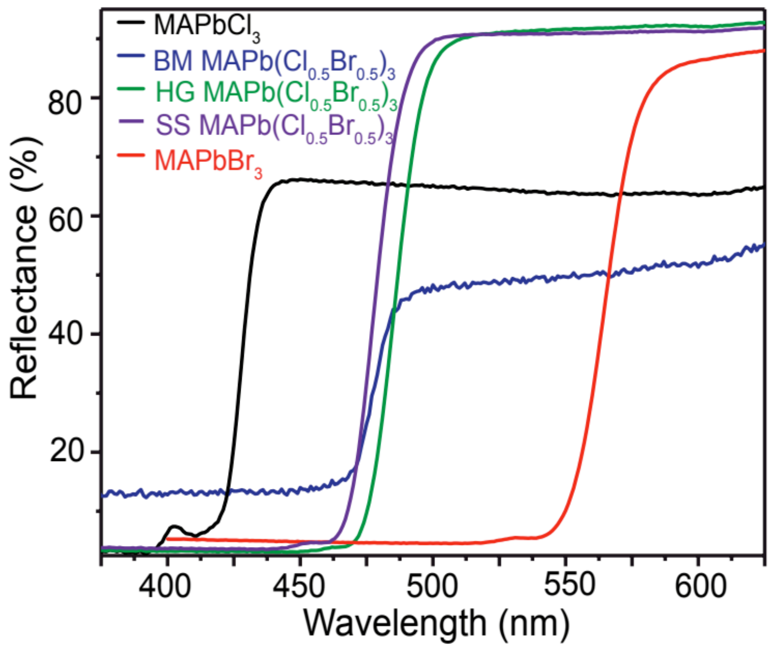

Figure S15. Diffuse reflectance spectra for MAPb(Cl$_{0.5}$Br$_{0.5}$)$_3$, prepared by BM, HG, and SS, along with those for the parent compounds, MAPbBr$_3$ and MAPbCl$_3$.

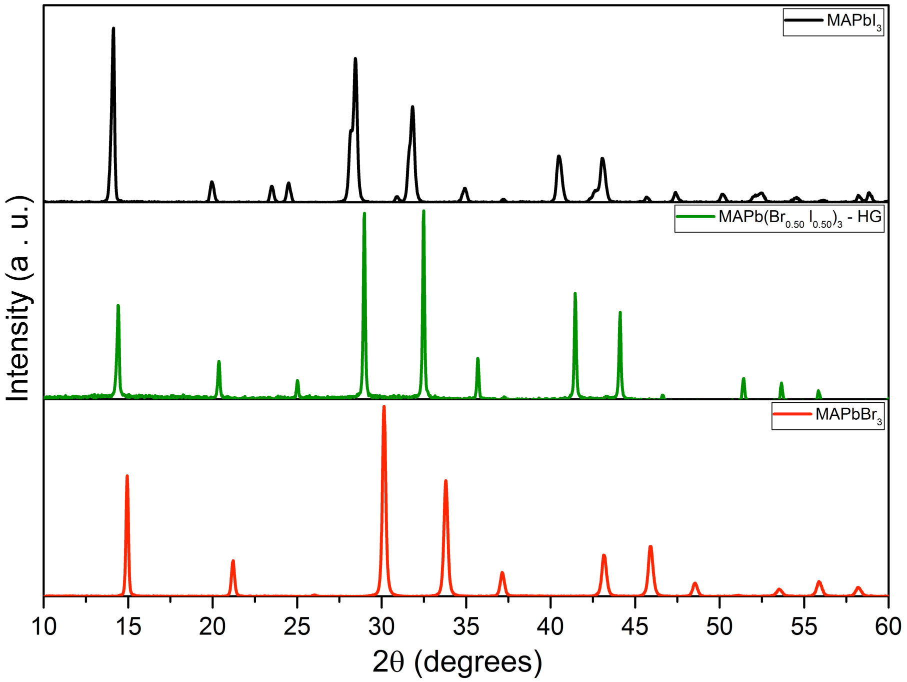

Figure S16. Comparison between XRD patterns of MAPb(Br$_{0.5}$I$_{0.5}$)$_3$ prepared by MCS-HG (2 hr) and those for the parent compounds, MAPbI$_3$ (tetragonal) and MAPbBr$_3$ (cubic).

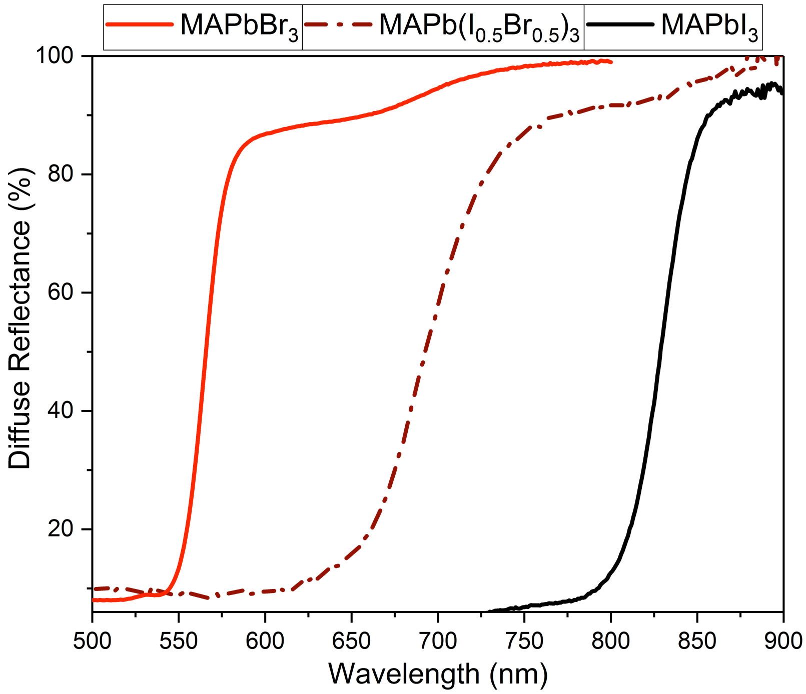

Figure S17. Diffuse reflectance spectra of the MAPb(Br$_{0.5}$I$_{0.5}$)$_3$ sample prepared by MCS-HG, along with those for the parent compounds, MAPbBr$_3$ and MAPbI$_3$.

References

---

[1] Roiland, C.; Trippe-Allard, G.; Jemli, K.; Alonso, B.; Ameline, J.-C.; Gautier, R.; Bataille, T.; Le Polles, L.; Deleporte, E.; Even, J., *et al.*, Multinuclear NMR as a Tool for Studying Local Order and Dynamics in $CH_3NH_3PbX_3$ (X = Cl, Br, I) Hybrid Perovskites. *Phys. Chem. Chem. Phys.* **2016,** *18* (39), 27133-27142.

[2] Rosales, B. A.; Men, L.; Cady, S. D.; Hanrahan, M. P.; Rossini, A. J.; Vela, J., Persistent Dopants and Phase Segregation in Organolead Mixed-Halide Perovskites. *Chem. Mater.* **2016,** *28* (19), 6848-6859.

[3] Burger, M. R.; Kramer, J.; Chermette, H.; Koch, K. R. A Comparison of Experimental and DFT Calculations of ^{195}Pt NMR Shielding Trends for $[PtX_nY_{6-n}]^{2-}$ (X, = Cl, Br, F, and I) Anions. *Magn. Reson. Chem.* **2010**, *48*, S38–S47.

[4] Fowe, E. P.; Belser, P. Daul, C.; Chermette, H. Assessment of Theoretical Prediction of the NMR Shielding Tensor of $^{195}PtCl_xBr_{6-x}{}^{2-}$ Complexes by DFT Calculations: Experimental and Computational Results. *Phys. Chem. Chem. Phys.* **2005**, *7*, 1732–1738.